Mono- And hexa-palladium doped silver nanoclusters stabilized by dithiolates

Subrat Kumar Barik, Tzu-Hao Chiu, Yu-Chiao Liu, Ming-Hsi Chiang, Franck Gam, Isaac Chantrenne, Samia Kahlal, Jean-Yves Saillard, C.W. Liu

COMMUNICATION

Mono- and hexa-palladium doped silver nanoclusters stabilized by dithiolates

Subrat Kumar Barik,[a] Tzu-Hao Chiu,[a] Yu-Chiao Liu,[b] Ming-Hsi Chiang,*[b] Franck Gam,[c] Isaac Chantrenne,[c] Samia Kahlal,[c] Jean-Yves Saillard,*[c] and C. W. Liu*[a]

The synthesis via a co-reduction method of the first Pd-containing silver-rich 21-metal-atom nanocluster passivated by dithiolates, $[PdAg_{20}\{S_2P(O^nPr)_2\}_{12}]$ (1), is reported. 1 is an 8 electron superatom isoelectronic to $[Ag_{21}\{S_2P(O^iPr)_2\}_{12}]^+$. Doping of Pd in 1 leads to its high stability against degradation in solution and shows a red emission in MeTHF at 77 K. In addition, we report a multi palladium doped silver nanocluster, $[Pd_6Ag_{14}(S)\{S_2P(O^nPr)_2\}_{12}]$ (2) for the first time. Its X-ray structure exhibits a sulfide-centered Pd_6Ag_2 rhombohedron surrounded by tweleve additional silver atoms with S_6 symmetry. XPS study and DFT calculations indicate that 2 contains Pd(0) and Ag(I) metals. A significant decrease in the electrochemical gap was observed in the SWVs of 2.

Introduction

Over the past few years, atomically and structurally precise bimetallic alloy nanoclusters (NCs) have engrossed substantial research interest owing to their synergetic and enhanced optical,[1] catalytic,[2] and electrochemical[3] properties compared with their homometallic counterparts of which related new advances should be also noted.[4] In this context, several structurally precise alloy NCs were produced from $Au_{25}(SR)_{18}$ via doping of Pd,[2e,5] Pt,[2a,6] Cd,[7] Hg,[8] Cu,[9] and Ag.[10] In particular, the studies unraveled that the doping of $[Au_{25}(SR)_{18}]^-$ with a single Pd or Pt atom not only increases cluster stability but also drastically enhances catalytic efficiency.[2a,e]

In case of silver, owing to its instability limitation (oxidation), only a handful of doped Ag NCs such as MAg_{24} (M = Pd or Pt),[11] Pt_2Ag_{23},[12] $PtAg_{28}$,[13] $PtAg_{42}$,[14] and $PtAg_{26}$,[15] have been structurally characterized. In addition, AuAg and other alloy NCs[16] also have been documented to achieve improved catalytic and optical properties. For example, Wu and co-workers showed significant tuning in the structural and photoluminescence properties via doping of Pd/Pt/Au atoms into $Ag_{25}(SR)_{18}$ (SR = 2,4-dimethylbenzenethiolate) NC.[17] Recently, Zhu *et al*.[2b] revealed that the central doping of Pd, Pt or Au into an Ag_{25} cluster has a significant influence on the catalytic performance in the carboxylation reaction of CO_2 with terminal alkyne through C-C bond formation. Given the prominence of Pd doped noble metal NCs, it is indeed extremely essential to generate different sizes of Pd-doped Ag clusters and thus to study their structure/property correlation. Surprisingly, only one anionic mono palladium doped Ag NC with different thiolates has been structurally characterized till date: $[PdAg_{24}(SR)_{18}]^{2-}$.[1a,11] This is largely due to the challenge of discriminating Pd from Ag since their atomic masses differ by merely 1.45 Da. Note that, an attempt to isolate Pd doped Ag NC by Chen *et al*. culminated in the synthesis of Ag_{33} NC rather than the doped one of late.[18] As a part of research on heavy atom doping on Ag and Cu NCs, we have recently produced structurally precise alloy NCs $[AuAg_{19}\{S_2P(O^nPr)_2\}_{12}]$,[19] $[AuAg_{20}\{Se_2P(OEt)_2\}_{12}]^+$[20] and $[PdCu_{14}H_2\{S_2CN^nBu_2/S_2P(O^iPr)_2\}_6(C{\equiv}CPh)_6]$.[21] in this study we isolated two unprecedented 21 and 20 metal based Pd doped Ag NCs $[PdAg_{20}\{S_2P(O^nPr)_2\}_{12}]$ (**1**) and $[Pd_6Ag_{14}(S)\{S_2P(O^nPr)_2\}_{12}]$ (**2**), respectively. The results provide that the cluster **2** is the first evidence of multi palladium doped Ag NC characterized by single-crystal X-ray diffraction study.

Results and discussion

In a typical one pot synthetic method, co-reduction of metal precursors $[Ag(CH_3CN)_4](PF_6)$ and $[Pd\{S_2P(O^nPr)_2\}_2]$ in the presence of $NH_4[S_2P(O^nPr)_2]$ using $LiBH_4{\cdot}THF$ as a reducing agent resulted in the isolation of $[PdAg_{20}\{S_2P(O^nPr)_2\}_{12}]$ (**1**) as brown red solids in 34 % yield (Scheme S1, ESI†). **1** was characterized by UV-vis, ^{31}P and ^1H NMR spectroscopy, ESI mass spectrometry, and and X-ray photoelectron spectroscopy (XPS). Its ^{31}P NMR spectrum shows a signal at 104.9 ppm at

[a] Department of Chemistry, National Dong Hwa University
No. 1 Sec. 2, Da Hsueh Rd., Shoufeng, Hualien 97401, Taiwan (R.O.C.)
E-mail: chenwei@mail.ndhu.edu.tw
Homepage: http://faculty.ndhu.edu.tw/~cwl/index.htm
[b] Institute of Chemistry, Academia Sinica
Taipei, 11528, Taiwan (R.O.C.)
[c] Univ Rennes, CNRS, ISCR-UMR 6226, F-35000 Rennes, France
E-mail: jean-yves.saillard@univ-rennes1.fr

† Electronic Supplementary Information (ESI) available: Experimental data, variable temperature NMR spectra (^{31}P), cyclic voltammetry, XPS and theoretical data of **1** and **2**. See DOI: 10.1039/x0xx00000x

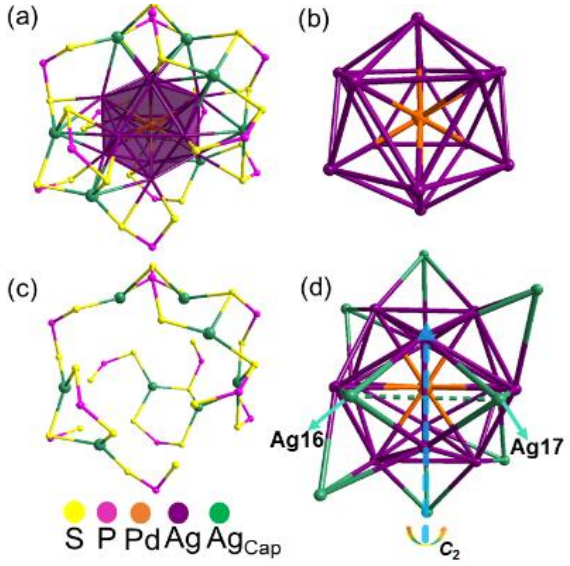

Fig. 1 (a) Total structure of $[PdAg_{20}\{S_2P(O^nPr)_2\}_{12}]$ (**1**) (propoxy groups omitted for clarity) (b) Pd@Ag_{12} icosahedron core without capping Ag atoms; dtp ligands omitted for clarity. (c) The capping silver atoms connected with 12 dtp ligands surrounding Pd@Ag_{12} icosahedron. (d) The pseudo-C_2 axis in the $PdAg_{20}$ framework.

room temperature (Fig. S1, ESI†) and ^{1}H NMR spectrum shows signals corresponding to ^{n}Pr group (Fig. S2, ESI†). Thus both ^{31}P and ^{1}H NMR spectra confirm the presence of di-propyl dithiophosphate (dtp) ligands in the cluster. The positive-ion ESI mass spectrum of **1** displays a prominent band corresponding to $[\mathbf{1}+Ag]^+$ at *m/z* 4930.8 (calcd. 4930.9), and its simulated isotopic pattern matches well with the experimental observation (Fig. S3, ESI†). **1** crystallizes in the monoclinic $P2_1/c$ space group. Its solid state structure unveiled a centered icosahedral Pd@Ag_{12} core stabilized by 8 capping Ag atoms and 12 dtp ligands (Fig. 1). This makes **1** a new member of the 8-electron $[MAg_{20}\{E_2P(OR)_2\}_{12}]^+$ (M = Ag, Au; E = S, Se; R = ^{i}Pr, Et) family.[20,22,23] However, **1** differs from its congeners with respect to the configuration of the 8 capping silvers, which confers to the M_{21} core an unprecedented idealized C_2 symmetry (Fig. 1a-c and Fig. S4, ESI†), whereas only T_h and D_3 core symmetries are known so far. [20,22] It has been shown that these different decorations around the icosahedral core are close in energy.[24] Their origination is likely the result of subtle (steric or kinetic) factors. Considering the ligands, the whole molecular symmetry of **1** is C_1.

The twelve dtp ligands are equally distributed in three layers (top, middle and bottom) around the pseudo-C_2 axis (Fig. 1c and Fig. S4, ESI†). They are coordinated to both capping and icosahedral silver atoms (Ag_{cap} and Ag_{ico}, respectively) in four binding modes in a ratio of 2:4:4:2; bimetallic triconnectivity (η^2: μ_2, μ_1), trimetallic triconnectivity (η^3: μ_2, μ_1), trimetallic tetraconnectivity (η^3: μ_2, μ_2) and tetrametallic tetraconnectivity (η^4: μ_2, μ_2) (Fig. S5, ESI†). The average Ag_{ico}-S (2.687 Å) and Ag_{cap}-S (2.540 Å) distances are analogous to those observed in $[Ag_{21}\{S_2P(O^iPr)_2\}_{12}]^+$ (hereon Ag_{21}) (2.670 Å and Ag_{cap} = 2.510 Å, respectively).[22] The existence of four types of dtp coordination environment in the X-ray structure encouraged us to investigate the variable temperature (VT) ^{31}P NMR spectrum of **1**. As the temperature was lowered from room temperature (RT) to -40 °C, the signal at 103.9 ppm split into four resonances at 106.5, 104.9, 104.5 and 103.7 ppm (Fig. S6, ESI†). Further lowering of temperature resulted in peak sharpening. This solution behaviour is consistent with the X-ray results.

The high-resolution X-ray photoelectron spectroscopy (XPS) spectrum of **1** in the Pd 3d region reveals binding energies at 335.9 and 341.1 eV, corresponding to Pd(0) $3d_{5/2}$ and $3d_{3/2}$ respectively (Fig. S7, ESI†). In comparison to its homometallic analogue Ag_{21},[22] As expected, the incoporation of Pd in **1** leads to doping-induced charge stripping phenomenon.[25]

DFT calculations[26] on a simplified model for **1**, $[PdAg_{20}\{S_2PH_2\}_{12}]$ (**1'**) shows an electronic structure related to that of previously reported isoelectronic M@Ag_{20} (M = Au, Ag) species.[20,22] In other words, **1** can be formally described as an 8-electron $[PdAg_{12}]^{4+}$ superatomic core passivated by eight Ag^+ and twelve dtp^- ions. The occupation of the icosahedron center by Pd is computed to be preferred over any of the other metallic positions by more than 20 kcal/mol. This result was already found for an Au-doped isoelectronic relative of **1**.[20a] This is related to the heteroatom electronegativity which is larger than that of Ag. The preference for Pd occupying the icosahedron center (by more than 20 kcal/mol) is related to its larger electronegativity than that of Ag. Indeed, replacing Pd

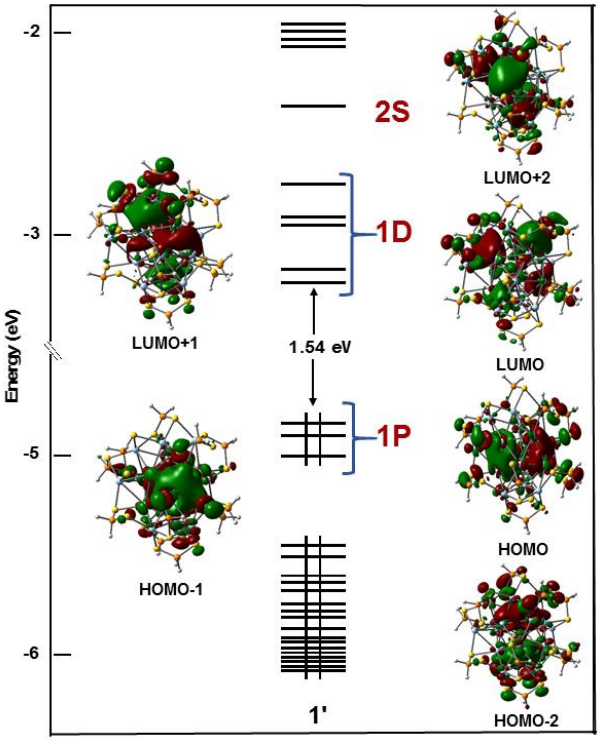

Fig. 2 Kohn-Sham molecular orbital diagram of **1'**.

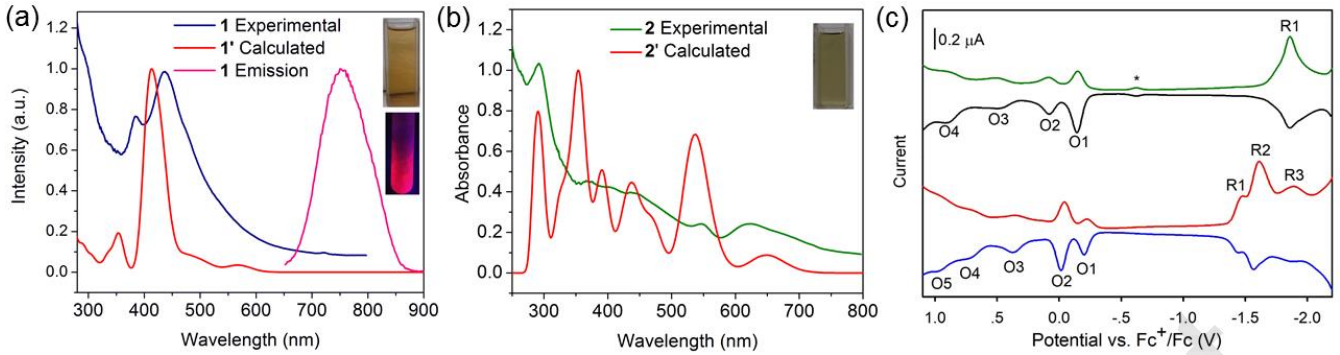

Fig. 3 (a) UV–vis spectrum (left) of **1** in 1 x 10^{-5} M CH_2Cl_2 and normalized emission spectrum (right) of **1** in MeTHF at 77 K. The TD-DFT-simulated spectrum of **1'** is superimposed in red. The insets show the photograph of solution of **1** in CH_2Cl_2 at room temperature (top) and 2-Methyl THF under UV irradiation at 77 K (bottom). (b) UV–vis spectrum of **2** in 1 x 10^{-5} M CH_2Cl_2 and the TD-DFT-simulated spectrum of **2'**.The inset shows the photograph of solution of **2** in CH_2Cl_2 at room temperature. (c) SWVs of **1** (top) and **2** (bottom) recorded in CH_2Cl_2 at 233K. Internal reference decamethylferrocene is denoted by an asterisk.

by Ag^+ in **1'**, leads to (averaged) natural atomic orbital (NAO) charges of -0.44, +0.20, and +0.58 for Ag_{center}, Ag_{ico} and Ag_{cap}, respectively, indicating that the electron-rich central position is strongly favored for Pd occupation. The computed NAO charges for **1'** are -0.99, +0.20, and +0.57 for Pd, Ag_{ico} and Ag_{cap}, respectively. They are in line with the XPS results. The MO diagram of **1'** is shown in Fig. 2. The three highest occupied and five lowest unoccupied orbitals can be viewed as the superatomic 1P and 1D levels, respectively (with some external shell admixture) whereas the LUMO+6 can be identified as the 2S level.

The UV-vis spectrum of **1** shows two major broad absorption bands at 384 and 436 nm (Fig. 3a). The absorption spectrum of **1** recorded in CH_2Cl_2 at 25 °C remains unchanged for a month (Fig. S8 ESI†) indicating high stability. The simulated TD-DFT[26] spectrum of **1'** (Fig. 3a) exhibits also two major band at 353 and 413 nm which can be attributed to metal-to-metal charge transfer (MMCT) 1P→2S and 1P→1D transitions. **1** displays photoluminescence in solution at cryogenic temperature. Its emission maximum in 2-methyl tetrahydrofuran (MeTHF) at 77 K occurs at 748 nm (Fig. 3a and Fig. S9, ESI†). The intensity decreases sharply upon raising the temperature to 298 K (Fig. S10, ESI†).

Cyclic voltammetry (CV) and square wave voltammetry (SWV) of **1** were performed in CH_2Cl_2 at various temperatures (Fig. 3c, and Fig. S11-S12, ESI†). The cyclic voltammogram at 233 K displays an irreversible reduction at E_{pc} = –1.97 V (vs. Fc^+/Fc) and four quasi reversible oxidation processes at $E_{1/2}$ = 0.12, 0.09, 0.52 and 0.91 V (Fig. S11, ESI†). Accordingly, the square wave voltammogram at 233K showed four oxidation peaks at -0.15 (O1), 0.09 (O2), 0.51 (O3), and 0.90 (O4) and one reduction peak at -1.86 V (Fig. 3c). The first oxidation and reduction peaks correspond to $[\mathbf{1}]^{+1/0}$ (O1) and $[\mathbf{1}]^{0/-1}$ (R1). The electrochemical HOMO-LUMO gap, which is the difference between O1 and R1, is calculated to be 1.71 eV for **1**. *To our knowledge, this is the first CVs/SWVs report of palladium doped silver NC*. The calculated value for this electrochemical gap[26] (1.46 eV), for **1'** agrees well with experiment.

In an attempt to synthesize multi-palladium-doped silver clusters we have isolated $[Pd_6Ag_{14}(S)\{S_2P(O^nPr)_2\}_{12}]$ (**2**) in 22% yield, along with **1** by increasing the $[Pd\{S_2P(O^nPr)_2\}_2]$ amount (Scheme S2, ESI†). **2** was purified by thin layer chromatography. It crystallizes in the triclinic *P(-)*1 space group. Its X-ray structure exhibits a sulfide-centered Pd_6Ag_{14} metallic framework protected by 12 dtp ligands with an idealized S_6 symmetry (Fig. 4a-c, and Fig. S13, ESI†). It can be visualized as a distorted Pd_6Ag_2 (Ag = Ag_A) rhombohedron; the faces of which are capped by six Ag_B atoms (Fig. 4d and 4e). Furthermore, this hexacapped rhombohedron has its six $Ag_BPdPdAg_B$ butterflies capped by six additional Ag_C atoms (Fig. 4e and 4f). Thus, the structure of **2** is completely different from that of **1** and related 8-electron species.[20,22,23]

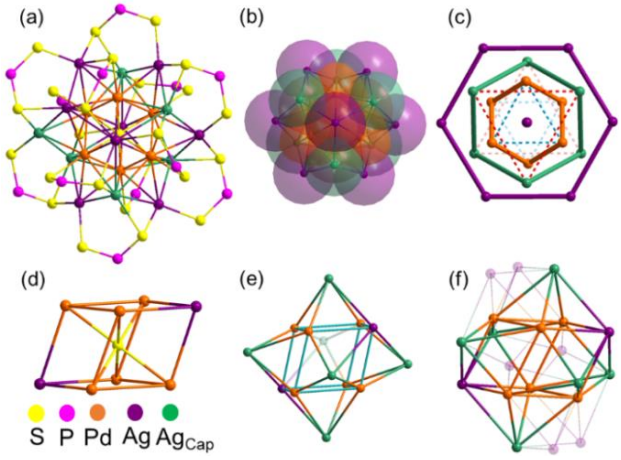

Fig. 4 (a) Total structure of $[Pd_6Ag_{14}S\{S_2P(O^nPr)_2\}_{12}]$ (**2**) with propoxy groups omitted for clarity. (b) The Pd_6Ag_{14} core. (c) View of the Pd_6Ag_{14} core along the C_3 axis. (d) The sulfide-rhombohedron. (f) The whole Pd_6Ag_{14} metal framework.

The encapsulated sulfur atom is connected to the six Pd centers in a distorted octahedral coordination mode (average Pd-S distance: 2.271(7) Å). *Surprisingly, there has been no*

example where sulfur is coordinated to six Pd atoms. The Pd-Pd distances (2.9088(5)-2.9293(5) Å) are longer those in bulk Pd (ca. Pd-Pd = 2.76 Å).[27] The $Ag_{A,B}$-Pd (2.7672(5) - 3.1903(5) Å) and $Ag_{A,B}$-$Ag_{A,B}$ (3.3017(5) - 3.2464(5) Å) distances are longer than those involving the Ag_C atoms (Ag_C-Pd: 2.8452(6) - 2.8733(6) Å) and Ag_C-Ag_C (2.8808(6) - 2.9627(6) Å). *To the best of our knowledge* ***2*** *is the first example among the noble metal clusters where a hexapalladium core is entrapped inside an Ag cluster.*

The entire Pd_6Ag_{14} metallic core in **2** is wrapped by twelve dtp ligands which are equally distributed in two layers of six ligands (inner and outer) around the S_6 axis and coordinated in a trimetallic triconnectivity (η^3: μ_2, μ_1) and tetrametallic tetraconnectivity (η^4: μ_2, μ_2) fashion (Fig. S14, ESI†). The average Pd-S (2.370 Å) and Ag-S (2.648 Å) bond distances are in the range of that one would expect from the literature.[28] Discarding the various metal-metal contacts, Pd is linearly coordinated to two S atoms (including the sulfide), Ag_A is tricoordinated, whereas Ag_B and Ag_C are bicoordinated.

The ^{1}H NMR spectrum of **2** is consistent with the presence of the ^{n}Pr groups (Fig. S15, ESI†). The ^{31}P NMR spectrum of **2** shows two different signals, corresponding to the two types of coordination modes (Fig. S16, ESI†). Moreover, the ^{31}P VT NMR spectra of **2** show conservation of the two signals, indicating that the molecular structure is retained in solution (Fig. S17, ESI†). The positive-ion ESI mass spectrum of **2** also confirms its composition, with a prominent band for $[\mathbf{2}+Ag]^+$ at *m/z* 4848.2 (calcd. 4847.9) and its simulated isotopic pattern matches well with the experimental observation (Fig. S18, ESI†). The XPS spectrum of **2** in the Pd 3d region reveals binding energies at 335.6 and 340.7 eV, corresponding to Pd(0) $3d_{5/2}$ and $3d_{3/2}$, respectively (Fig. S19, ESI†).

DFT calculations on a simplified model for **2**,[26] $[Pd_6Ag_{14}(S)\{S_2PH)_2\}_{12}]$ (**2'**) supports the view of a cluster made up of d^{10} metal centers (Pd(0) and Ag(I)). The NAO charges of Pd, Ag_A, Ag_B and Ag_C are -0.30, +0.58, +0.49 and +0.57, respectively, that of the hypercoordinated central sulfide is -0.36, indicating important charge transfer to the Pd centers, thus substantial covalency. Consistently, the corresponding Pd-S Wiberg bond index (WBI) of 0.278 compares well with that of the Pd-S(dtp) bonds (0.335). The electron deficiency of the 16- and 14-electron centers (Ag_A and Pd, Ag_B and Ag_C, respectively) is partly compensated by weak metal-metal bonding associated with some 4d→4s/4p electron transfer. Indeed, the corresponding WBIs remain within the range of what is expected to occur for metallophilic d^{10}-d^{10} interactions[29] (Pd-Pd: 0.077; Ag-Ag range: 0.055-0.074; Ag-Pd range: 0.057-0.092).[30] This electron deficiency can be traced in the nature of the lowest unoccupied MOs (Fig. S20, ESI†), whereas the highest occupied MOs are 3d(Pd) combinations.

The absorption spectrum of **2** shows multiple bands in the range 290 to 620 nm and an intense band at 291 nm (Fig. 3b). The absorption spectrum recorded in CH_2Cl_2 at 25 °C remains unchanged for a month (Fig. S21, ESI†) indicating high stability. The simulated TD-DFT[26] spectrum of **2'** (Fig. 3b) agrees well with experiment. The low energy band is of palldium-to-silver charge transfer (PdAgCT) nature and the next one of Ag(d)Ag(sp)CT nature.

CVs and SWVs were also performed on **2** in CH_2Cl_2 at various temperatures (Fig. 3c, Fig. S22 and S23, ESI†). The cyclic voltammogram at 233 K displays three irreversible reductions at Epc = –1.47, –1.67 and –1.91 V. Four irreversible oxidations at Epa = –0.13, 0.45, 0.76, 1.01 V, and one quasi-reversible oxidation process at $E_{1/2}$ = –0.01 V were observed while the fifth oxidation process was clearly observed in the SWV. The corresponding values of the SWV were obtained at –1.48 (R1), –1.62 (R2), –1.89 (R3) for the cathodic events, and –0.20 (O1), –0.01 (O2), 0.38 (O3), 0.72 (O4), 0.97 (O5) for the anodic ones (Fig. 3c). Compared with **1**, **2** exhibits more reductions and oxidations in which they are much easier to be accessed. The resulting electrochemical HOMO-LUMO gap is decreased to 1.28 eV. Its DFT-computed counterpart calculated[26] for **2'** is also 1.28 eV.

During the course of synthesis of **2**, we also observe the formation of **1**, thus were interested to see the connection between **1** and **2**. As given in Scheme S2, we propose that the formation of **2** is associated with the redox reaction between the residual amount of Ag(0) formed in parallel to the formation of **1** with Pd(II) and S atom. Since, 2 Ag(0) can reduce one Pd(II) into Pd(0) and one S atom into S^{2-} independently, then **2** accommodates 14 Ag^+, 6 Pd^0 and 1 S^{2-} ions (Fig. S24, ESI†). Note that the sulfide is generated from a P-S bond cleavage of dtp ligand by the $LiBH_4$·THF reducing agent.

Conclusions

In conclusion, one pot synthesis and full characterization of the molecularly pure, charge neutral Pd doped silver NC $[PdAg_{20}\{S_2P(O^nPr)_2\}_{12}]$ is presented. It displays a Pd-centered Ag_{12} icosahedron capped by 8 silver atoms in C_2 symmetry. Apart from its high stability, **1** features red emission at cryogenic temperature and doping induced charge stripping. Additionally, we have isolated the Pd_6Ag_{14} bimetallic NC (**2**) in which an octahedral hexa-palladium(0) core is embodied within a silver(I) cluster, the first one in literature. Bonding characteristics of both alloys have been fully rationalized by DFT calculations and among them hexa-palladium doped silver NC displays a smaller electrochemical HOMO-LUMO gap. We anticipate that the isolation of these novel bimetallic NCs in their pure forms makes a new frontier in the alloy synthesis with enhanced synergistic properties for multiple potential applications such as C-C bond cross-coupling reactions.

Conflicts of interest

There are no conflicts to declare.

Acknowledgements

This work was supported by the Ministry of Science and Technology in Taiwan (MOST 106-2113-M-259-010). The ANR-MOST 2018

program (project Nanoalloys) and the GENCI computer resource center (grant A0030807367).

Notes and references

1 (a) M. S. Bootharaju, C. P. Joshi, M. R. Parida, O. F. Mohammed and O. M. Bakr, *Angew. Chem., Int. Ed.,* 2016, **55**, 922-926; (b) R. P. B. Silalahi, K. K. Chakrahari, J.-H. Liao, S. Kahlal, Y.-C. Liu, M.-H. Chiang, J.-Y. Saillard and C. W. Liu, *Chem. Asian J.*, 2018, **13**, 500-504; (c) Z. Lei, X.-Y. Pei, Z.-G. Jiang and Q.-M. Wang, *Angew. Chem. Int. Ed.*, 2014, **53**, 12771-12775; (d) S. Wang, X. Meng, A. Das, T. Li, Y. Song, T. Cao, X. Zhu, M. Zhu and R. Jin, *Angew. Chem. Int. Ed.*, 2014, **53**, 2376-2380; (e) T. Udayabhaskararao, Y. Sun, N. Goswami, S. K. Pal, K. Balasubramanian and T. Pradeep, *Angew. Chem. Int. Ed.,* 2012, **51**, 2155-2159.

2 (a) H. Qian, D.-e. Jiang, G. Li, C. Gayathri, A. Das, R. R. Gil and R. Jin, *J. Am. Chem. Soc.*, 2012, **134**, 16159-16162; (b) Y. Liu, X. Chai, X. Cai, M. Chen, R. Jin, W. Ding and Y. Zhu, *Angew. Chem. Int. Ed.,* 2018, **57**, 9775-9779; (c) C. Yao, J. Chen, M.-B. Li, L. Liu, J. Yang and Z. Wu, *Nano Lett.*, 2015, **15**, 1281-1287; (d) S. Wang, S. Jin, S. Yang, S. Chen, Y. Song. J. Zhang and M. Zhu, *Sci. Adv.*, 2015, 1:e1500441; (e) S. Xie, H. Tsunoyama, W. Kurashige, Y. Negishi and T. Tsukuda, *ACS Catal.*, 2012, **2**, 1519-1523.

3 (a) C. A. Fields-Zinna, M. C. Crowe, A. Dass, J. E. F. Weaver and R. W. Murray, *Langmuir*, 2009, **25**, 7704-7710; (b) K. Kwak, Q. Tang, M. Kim, D.-e. Jiang and D. Lee, *J. Am. Chem. Soc.* 2015, **137**, 10833-10840; (c) L. Liao, S. Zhou, Y. Dai, L. Liu, C. Yao, C. Fu, J. Yang and Z. Wu, *J. Am. Chem. Soc.* 2015, **137**, 9511-9514; (d) J.-P. Choi, C. A. Fields-Zinna, R. L. Stiles, R. Balasubramanian, A. D. Douglas, M. C. Crowe and R. W. Murray, *J. Phys. Chem. C*, 2010, **114**, 15890-15896.

4 (a) Z. Wang, H.-F. Su, M. Kurmoo, C.-H. Tung, D. Sun and L.-S. Zheng, *Nat. Commun.*, 2018, **9**, 2094-2101; (b) J.-Y. Liu, F. Alkan, Z. Wang, Z.-Y. Zhang, M. Kurmoo, Z. Yan, Q.-Q. Zhao, C. M. Aikens, C.-H. Tung and D. Sun, *Angew. Chem. Int. Ed.* 2019, **58**, 195-199; (c) S.-F. Yuan, C.-Q. Xu, J. Li and Q.-M. Wang, *Angew. Chem. Int. Ed.,* 2019, **58**, 5906-5909; (d) J.-W. Liu, Z. Wang, Y.-M. Chai, M. Kurmoo, Q.-Q. Zhao, X.-P. Wang, C.-H. Tung and D. Sun, *Angew. Chem. Int. Ed.* 2019, **58**, 6276 6279; (e) S.-S. Zhang, F. Alkan, H.-F. Su, C. M. Aikens, C.-H. Tung and D. Sun, *J. Am. Chem. Soc.,* 2019, **141**, 4460-4467.

5 (a) Y. Negishi, W. Kurashige, Y. Niihori, T. Iwasa and K. Nobusada, *Phys. Chem. Chem. Phys.* 2010, **12**, 6219-6225; (b) Y. Negishi, K. Igarashi, K. Munakata, W. Ohgake, K. Nobusada, *Chem. Commun.*, 2012, **48**, 660-662.

6 S. L. Christensen, M. A. MacDonald, A. Chatt, P. Zhang, H. Qian and R. Jin, *J. Phys. Chem. C*, 2012, **116**, 26932-26937.

7 S. Wang, Y. Song, S. Jin, X. Liu, J. Zhang, Y. Pei, X. Meng, M. Chen, P. Li and M. Zhu, *J. Am. Chem. Soc.* 2015, **137**, 4018-4021.

8 L. Liao, S. Zhou, Y. Dai, L. Liu, C. Yao, C. Fu, J. Yang and Z. Wu, *J. Am. Chem. Soc.,* 2015, **137**, 9511-9514.

9 Y. Negishi, K. Munakata, W. Ohgake and K. Nobusada, *J. Phys. Chem. Lett.*, 2012, **3**, 2209-2214.

10 (a) Y. Negishi, T. Iwai and M. Ide, *Chem. Commun.,* 2010, **46**, 4713-4715; (b) C. Kumara, C. M. Aikens and A. J. Dass, *Phys. Chem. Lett.,* 2014, **5**, 461-466; (c) D. R. Kauffman, D. Alfonso, C. Matranga, H. Qian and R. Jin, *J. Phys. Chem. C,* 2013, **117**, 7914-7923.

11 J. Yan, H. Su, H. Yang, S. Malola, S. Lin, H. Hakkinen and N. Zheng, *J. Am. Chem. Soc.* 2015, **137**, 11880-11883.

12 M. S. Bootharaju, S. M. Kozlov, Z. Cao, M. Harb, N. Maity, A. Shkurenko, M. R. Parida, M. N. Hedhili, M. Eddaoudi, O. F. Mohammed, O. M. Bakr, L. Cavallo and J.-M. Basset, *J. Am. Chem. Soc.*, 2017, **139**, 1053-1056.

13 (a) M. S. Bootharaju, S. M. Kozlov, Z. Cao, A. Shkurenko, A. M. El-Zohry, O. F. Mohammed, M. Eddaoudi, O. M. Bakr, L. Cavallo and J.-M. Basset, *Chem. Mater.,* 2018, **30**, 2719-2725; (b) X. Lin, C. Liu, K. Sun, R. Wu, X. Fu and J. Huang, *Nano Res.*, 2019, **12**, 309-314.

14 H. Shen and T. Mizuta, *Chem. Asian J.*, 2017, **12**, 2904-2907.

15 L. Z. He, J. Y. Yuan, N. Xia, L. W. Liao, X. Liu, Z. B. Gan, C. M. Wang, J. L. Yang and Z. K. Wu, *J. Am. Chem. Soc.,* 2018, **140**, 3487-3490.

16 N. Yan, L. Liao, J. Yuan, Y.-j. Lin, L.-h. Weng, J. Yang and Z. Wu, *Chem. Mater.,* 2016, **28**, 8240-8247.

17 X. Liu, J. Yuan, C. Yao, J. Chen, L. Li, X. Bao, J. Yang and Z. Wu. *J. Phys. Chem. C*, 2017, **121**, 13848-13853.

18 F. Tian and R. Chen, *J. Am. Chem. Soc.*, 2019, 10.1021/jacs.9b02162.

19 Y.-R. Lin, P. V. V. N. Kishore, J.-H. Liao, S. Kahlal, Y.-C. Liu, M.-H. Chiang, J.-Y. Saillard and C. W. Liu, *Nanoscale,* 2018, **10**, 6855-6860.

20 (a) W.-T. Chang, P.-Y. Lee, J.-H. Liao, K. K. Chakrahari, S. Kahlal, Y.-C. Liu, M.-H. Chiang, J.-Y. Saillard and C. W. Liu, *Angew. Chem. Int. Ed*., 2017, **56**, 10178-10182; (b) J.-H. Liao, S. Kahlal, Y.-C. Liu, M.-H. Chiang, J.-Y. Saillard and C. W. Liu, *J. Clust. Sci.* 2018, **29**, 827-835.

21 K. K. Chakrahari, R. P. B. Silalahi, T.-H. Chiu, X. Wang, N. Azrou, S. Kahlal, Y. -C. Liu, M.-H. Chiang, J.-Y. Saillard and C. W. Liu, *Angew. Chem. Int. Ed.,* 2019, **58**, 4943-4947.

22 R. S. Dhayal, J.-H. Liao, Y.-C. Liu, M.-H. Chiang, S. Kahlal, J.-Y. Saillard and C. W. Liu, *Angew. Chem. Int. Ed.,* 2015, **54**, 3702-3706.

23 S. Sharma, K. K. Chakrahari, J.-Y. Saillard and C. W. Liu, *Acc. Chem. Res.,* 2018, **51**, 2475-2483.

24 R. S. Dhayal, Y.-R. Lin, J.-H. Liao, Y.-J. Chen, Y.-C. Liu, M.-H. Chiang, S. Kahlal, J.-Y. Saillard and C. W. Liu, *Chem. Eur. J.*, 2016, **22**, 9943-9947.

25 A. Ghosh, O. F. Mohammed and O. M. Bakr, *Acc. Chem. Res.* 2018, **51**, 3094-3103.

26 Computational details in the SI.

27 (a) T. Murahashi, H. Kurosawa, Coord. Chem. Rev. 2002, 231, 207-228; (b) M. Teramoto, K. Iwata, H. Yamaura, K. Kurashima, K. Miyazawa, Y. Kurashige, K. Yamamoto and T. Murahashi, *J. Am. Chem. Soc.*, 2018, **140**, 12682-12686.

28 Y.-J. Kim, K.-Y. Choi, S. G. Lee, Z. N. Zheng and S. W. Lee, *Bull. Korean Chem. Soc.*, 2014, **35**, 1205-1208.

29 C. W. Liu, P.-K. Liao, C.-S. Fang, J.-Y. Saillard, S. Kahlal and J.-C. Wang, *Chem. Commun.*, 2011, **47**, 5831-5833.

30 Introducing dispersion corrections slightly strengthens d^{10}-d^{10} bonding (Table S2).